# CEACAM1: a key regulator of vascular permeability

**Anne-Laure Nouvion[1], Malika Oubaha[2], Sarah LeBlanc[1], Elaine C. Davis[3], Holger Jastrow[4], Robert Kammerer[5], Valérie Breton[1], Claire Turbide[1], Suleyman Ergun[3,*], Jean-Philippe Gratton[2,*] and Nicole Beauchemin[1,6,‡]**

[1]Goodman Cancer Research Centre, McGill University, Montreal, QC H3G 1Y6, Canada
[2]Laboratory of Endothelial Cell Biology, Institut de Recherches Cliniques de Montréal, Université de Montréal, Montréal, QC H2W 2T2, Canada
[3]Department of Anatomy and Cell Biology, McGill University, Montreal, QC H3A 2B2, Canada
[4]Institute of Anatomy, University Hospital Essen, Essen 45147, Germany
[5]Institute of Immunology, Friedrich-Loeffler-Institute, Tuebingen 72076, Germany
[6]Departments of Biochemistry, Medicine and Oncology, McGill University, Montreal, QC H3G 1Y6, Canada
*These authors contributed equally to this work
‡Author for correspondence (nicole.beauchemin@mcgill.ca)

*Accepted 23 August 2010*
*Journal of Cell Science 123, 4221-4230*

*doi:10.1242/jcs.073635*

## Summary

Carcinoembryonic antigen cell adhesion molecule-1 (CEACAM1) is an immunoglobulin-like cell surface co-receptor expressed on epithelial, hematopoietic and endothelial cells. CEACAM1 functions as an adhesion molecule, mainly binding to itself or other members of the CEA family. We and others have previously shown that CEACAM1 is crucial for in vivo vascular integrity during ischemic neo-vascularization. Here, we have deciphered the roles of CEACAM1 in normal and pathological vascularization. We have found that *Ceacam1*–/– mice exhibit a significant increase in basal vascular permeability related to increased basal Akt and endothelial nitric oxide synthase (eNOS) activation in primary murine lung endothelial cells (MLECs). Moreover, CEACAM1 deletion in MLECs inhibits VEGF-mediated nitric oxide (NO) production, consistent with defective VEGF-dependent in vivo permeability in *Ceacam1*–/– mice. In addition, *Ceacam1*-null mice exhibit increased permeability of tumor vasculature. Finally, we demonstrate that CEACAM1 is tyrosine-phosphorylated upon VEGF treatment in a SHP-1- and Src-dependent manner, and that the key residues of the long cytoplasmic domain of CEACAM1 are crucial for CEACAM1 phosphorylation and NO production. This data represents the first report, to our knowledge, of a functional link between CEACAM1 and the VEGFR2/Akt/eNOS-mediated vascular permeability pathway.

**Key words:** Cell adhesion, CEACAM1, Endothelial, Vascular permeability, Angiogenesis, eNOS, VEGFR2, SHP-1

## Introduction

Angiogenesis, the formation of new blood vessels from a pre-existing vascular bed, is a pivotal biological process not only during embryonic development and in physiological conditions, but also in a variety of pathological situations (Carmeliet, 2003). One of the most specific and crucial angiogenic regulators is vascular endothelial growth factor (VEGF). VEGF promotes angiogenesis by a number of mechanisms, including stimulation of endothelial cell proliferation and migration as well as increased vascular permeability (Olsson et al., 2006). Precise regulation of vascular permeability is essential for the health of normal tissues, and abnormal vascular permeability is an important characteristic of pathologies associated with angiogenesis such as tumor development (Nagy et al., 2008). Endothelium-derived nitric oxide (NO), originally identified as endothelium-derived relaxing factor, promotes angiogenesis and plays an important role in vascular remodeling, vascular permeability and the maintenance of vascular integrity (Sessa, 2004; Nagy et al., 2008). In endothelial cells (ECs), NO results from the conversion of L-arginine to citrulline by endothelial NO synthase (eNOS). eNOS produces low levels of NO constitutively, but can be transiently stimulated to produce high levels by various hormones and environmental stimuli such as VEGF. Indeed, VEGF causes NO production by ECs via PI3K/Akt-dependent eNOS activation (Sessa, 2004).

Carcinoembryonic antigen-related cell adhesion molecule-1 (CEACAM1/CD66a/Bgp) is a member of the immunoglobulin (Ig) superfamily. Murine and human CEACAM1 exhibit a heavily glycosylated extracytoplasmic region with two or four Ig-like domains, produced by alternative splicing. CEACAM1s are tethered to the membrane and contain either a short (10 amino acids, CEACAM1-S) or long (71–73 amino acids, CEACAM1-L) cytoplasmic domain. CEACAM1 is expressed in a wide range of cells including hematopoietic, epithelial and endothelial cells, where it exerts various biological functions that range from cell adhesion to cell signaling. It affects host immune responses and epithelial integrity as well as maintenance of homeostasis relative to cell proliferation and differentiation (Sadekova et al., 2000; Najjar, 2002; Poy et al., 2002; Fournes et al., 2003; Abou-Rjaily et al., 2004; Gray-Owen and Blumberg, 2006; Leung et al., 2006; Slevogt et al., 2008; Nouvion and Beauchemin, 2009).

We and others have reported that exogenously applied soluble CEACAM1 exhibits angiogenic properties and functions as a morphogenic effector for VEGF (Ergun et al., 2000). More importantly, we have shown that CEACAM1 plays a major role in vascular integrity and formation of the vascular network in vivo, particularly during normal neo-vascularization (Horst et al., 2006). Moreover, Muller and co-workers established that transmembrane CEACAM1-L expressed on endothelial cells was implicated in angiogenic activation by affecting cytoskeletal architecture and integrin-mediated signaling (Muller et al., 2005). Accordingly, CEACAM1 is expressed in newly formed vessels during physiological angiogenesis such as in wound healing and endometrial proliferation, as well as in immature new blood vessels of different tumors (Ergun et al., 2000; Kilic et al., 2005).

Downregulation of epithelial CEACAM1-L in prostate intraepithelial neoplasia (PIN) was accompanied by its upregulation in adjacent vasculature, which correlated with vascular destabilization and increased vascularization of prostate tumors (Tilki et al., 2006). Furthermore, endothelial expression of CEACAM1 activates signaling mechanisms promoting lymphatic reprogramming of vascular endothelial cells, suggesting that CEACAM1 might play a role in metastasis by increasing tumor lymphangiogenesis, and thus tumor access to lymphatic vessels (Kilic et al., 2007). Finally, it has recently been shown that CEACAM1 expression on myeloid cells controls angiogenesis in inflammation (Horst et al., 2009).

To conclusively assess the global impact of CECAM1 on angiogenesis, we interrogated the consequences of CEACAM1 deletion in the endothelial cell compartment. In this manuscript, we report that VEGF-induced signaling in *Ceacam1*-null primary murine lung endothelial cells (MLECs) exposes a defective eNOS signaling pathway with diminished NO production, and is consistent with defective acute VEGF-dependent in vivo permeability. Moreover, we show that systemic CEACAM1 elimination significantly enhances permeability of tumor vasculature as well as basal vascular permeability of lungs, skin and kidneys in vivo, a phenomenon that correlates with the increased basal Akt and eNOS phosphorylation levels in MLECs. Finally, we demonstrate that CEACAM1 is tyrosine-phosphorylated upon VEGF treatment in a SHP-1- and Src-dependent manner, and that the key residues of the ITIM motif of CEACAM1 are crucial for CEACAM1 phosphorylation and NO production. Taken together, these data constitute the first report, to our knowledge, of a functional link between CEACAM1 and the VEGFR2/Akt/eNOS-mediated vascular permeability pathway.

## Results

### CEACAM1 overexpression increases VEGFR2-mediated NO production whereas CEACAM1 knockdown inhibits it

Because CEACAM1 plays a major role in angiogenesis and vascular integrity (Ergun et al., 2000; Kilic et al., 2005; Muller et al., 2005; Horst et al., 2006; Tilki et al., 2006; Kilic et al., 2007; Horst et al., 2009), we questioned whether the vascular permeability pathway and, more specifically, the eNOS/Akt pathway was dysregulated by CEACAM1. We measured NO release from COS-7 cells co-transfected with CEACAM1-L or CEACAM1-S, eNOS and VEGFR2. Fig. 1A shows that CEACAM1-L coexpression with VEGFR2 and eNOS in COS-7 cells doubles the amounts of NO accumulated in the culture medium in response to VEGFR2 activation, compared with that of untransfected cells. Coexpression of CEACAM1-S did not affect NO production. This result demonstrates that expression of the long cytoplasmic domain isoform of CEACAM1 contributes to eNOS activity in a reconstituted system (COS-7). We then analyzed VEGF-induced NO production in endothelial cells, a cell type directly involved in angiogenesis process. MLECs were prepared from either wild-type (WT) or *Ceacam1*–/– mice and their purity assessed by uptake of di-acetylated LDL and immunoreactivity to CD31 antibody (supplementary material Fig. S1) and judged to be 96%. We first confirmed that MLECs exhibited endogenous expression of CEACAM1 by using RT-PCR, immunoprecipitation and immunostaining analyses and showed that both CEACAM1-S and CEACAM1-L isoforms are expressed in the WT primary endothelial cells (supplementary material Fig. S2). Subsequently, MLECs were stimulated for 30 minutes with VEGF and tested for NO production. Whereas VEGF treatment increased NO production in WT MLECs, induction of NO was completely deficient in

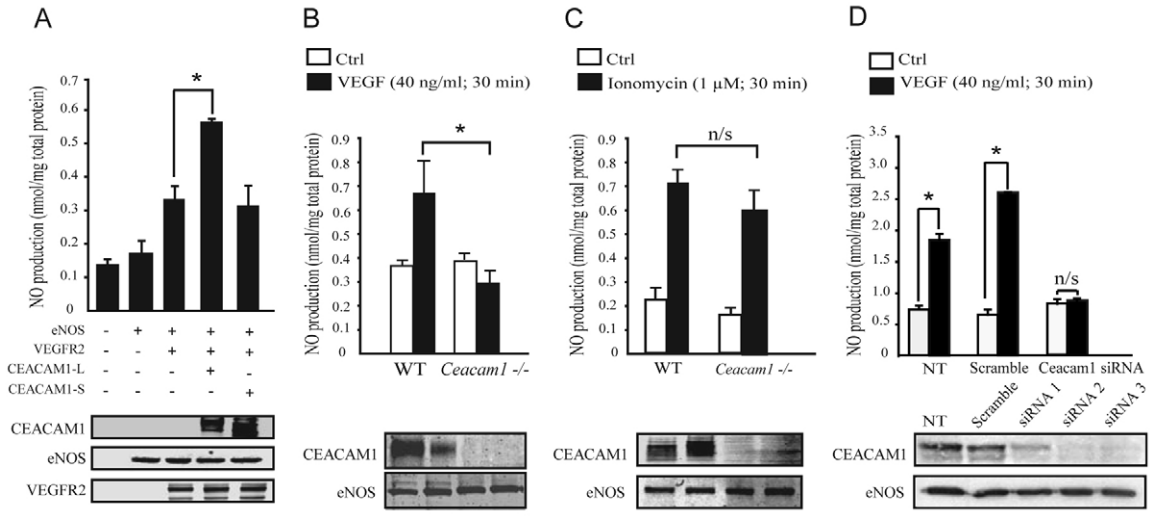


**Fig. 1. VEGFR2-mediated NO production is regulated by CEACAM1 expression.** (**A**) COS-7 cells were transfected with VEGFR-2, eNOS, CEACAM1-L or CEACAM1-S as indicated. At 48 hours after transfection, cell culture medium was processed for the measurement of NO as described in Materials and Methods. (**B**,**C**) MLECs were prepared from C57Bl/6 WT and *Ceacam1*–/– mice ($n$=3), serum-starved for 6 hours, and treated or not with (B) VEGF (40 ng/ml) for 30 minutes or (C) ionomycin (1 μM) for 30 minutes. Ctrl, control (untreated). Samples of culture media were taken for NO quantification. Data are the average + s.e.m. of at least four experiments. For each experiment shown in A, B and C, protein expression was verified. Cells were collected, lysed, and equal amounts of proteins were separated by PAGE gels and immunoblotted with rabbit anti-CEACAM1 Ab, anti-eNOS Ab or anti-VEGFR2 Ab. (**D**) BAECs were transfected with 100 pmol of either scrambled or three different *Ceacam1*-specific siRNAs (siRNA1, siRNA2, siRNA3); NT, non-transfected. After 48 hours, BAECs were treated for 30 minutes with 40 ng/ml of VEGF and processed for measurement of nitrite. The NO production for *Ceacam1*-specific siRNA-treated BAECs is the average of the three *Ceacam1*-specific siRNA-treated samples, each of them performed in duplicate. *$P$<0.05.

*Ceacam1–/–* MLECs (Fig. 1B). To determine whether this effect was VEGF-dependent and not due to impaired global eNOS activity and expression, the calcium ionophore ionomycin was used as a stimulus for NO production. eNOS protein levels were monitored in WT and *Ceacam1–/–* MLECs. Both WT and *Ceacam1–/–* MLECs displayed similar eNOS protein levels (Fig. 1C) and sustained a significant induction of NO production after ionomycin treatment compared to untreated controls ($P<0.05$).

To confirm that CEACAM1 knockdown inhibits VEGFR2-mediated NO production endogenously, we used small interfering RNA (siRNA) against bovine CEACAM1 in BAECs cells. Three siRNAs were tested and showed a partial or complete downregulation of bovine CEACAM1 (Fig. 1D). A scrambled siRNA and non-transfected cells were used as controls. Transfected BAECs were then stimulated for 30 minutes with VEGF and tested for NO production. Our results showed that downregulation of bovine CEACAM1 by siRNA completely abolished NO production after VEGF treatment (Fig. 1D). Taken together, these results demonstrate that CEACAM1 deficiency affects VEGF signaling via the eNOS pathway.

### VEGFR2-mediated eNOS activation is deficient in *Ceacam1–/–* primary MLECs

VEGF-mediated activation of VEGFR2 stimulates NO production through Akt-dependent eNOS phosphorylation of Ser1177 (Sessa, 2004). We therefore investigated whether CEACAM1 deletion impacted on eNOS and Akt activity by measuring eNOS Ser1177 and Akt Ser473 phosphorylation following VEGF treatment (Fig. 2A,B). eNOS phosphorylation was clearly augmented in WT MLECs after a 5-minute VEGF treatment, and this increased activity was sustained for 30 minutes. Accordingly, we detected an increase in Akt Ser473 phosphorylation after 5 and 10 minutes in WT MLECs. However, in *Ceacam1–/–* MLECs, basal phosphorylation of both eNOS and Akt proteins was significantly elevated before stimulation, and showed no further increase after VEGF treatment (Fig. 2A,B). Surprisingly, the results of Fig. 1 showed impaired eNOS activation and subsequent lack of NO production after VEGF treatment in *Ceacam1–/–* MLECs. To clarify these seemingly opposite results, we measured NO accumulation in both WT and *Ceacam1–/–* MLECs after culturing for 24 hours. Our results showed that NO accumulation was significantly higher in *Ceacam1–/–* MLECs compared with the WT (Fig. 2C), consistent with elevated basal phosphorylation levels of eNOS proteins before stimulation (Fig. 2A).

In addition to stimulating the Akt/eNOS pathway, VEGF signaling via VEGFR2 activates Erk, which generally results in EC proliferation. Accordingly, our results show that VEGF induced a time-dependent Erk1/2 phosphorylation in both WT and *Ceacam1–/–* MLECs with an approximately 1.5-fold induction of Erk1/2 activity after 5 minutes of VEGF stimulation (Fig. 2B). This suggests that endothelial CEACAM1 functions are Akt- and eNOS-dependent, but do not involve Erk-mediated pathways.

### CEACAM1 is tyrosine-phosphorylated upon VEGF treatment in a SHP-1- and Src-dependent manner

To further investigate the mechanisms involved in the modulation of signaling downstream of VEGFR2 by CEACAM1, we questioned whether this involved the CEACAM1 long cytoplasmic domain, because only CEACAM1-L expressing cells responded to VEGF2 activation (Fig. 1A). This cytoplasmic tail contains an immunoreceptor tyrosine-based inhibition motif (ITIM) that mediates interactions with other intracellular proteins in a phosphorylation-dependent manner. Previous studies have shown that tyrosine phosphorylation of CEACAM1-L within the ITIM motif is crucial for its function, including the regulation of signaling pathways in epithelial and immune cells (Huber et al., 1999; Izzi et al., 1999). Upon tyrosine phosphorylation, CEACAM1-L can bind SH2 domain-containing proteins, thereby activating Src-family tyrosine kinases and the protein tyrosine phosphatases SHP-1 and SHP-2 (Huber et al., 1999; Poy et al., 2002; Dubois et al., 2006; Chen et al., 2008; Klaile et al., 2009; Muller et al., 2009). We therefore evaluated whether CEACAM1-L was phosphorylated in response to VEGF treatment of endothelial cells and whether SHP-1 and the Src-like kinases played a role in CEACAM1-mediated endothelial phenotypes. To address this, bovine aortic endothelial cells (BAECs) were transfected with murine CEACAM1-L and treated with VEGF for 3 minutes (Fig. 3A). Cells were lysed and proteins were immunoprecipitated with an anti-phosphotyrosine antibody. Blotting with a VEGFR2-specific antibody confirmed its phosphorylation and therefore its activation following VEGF treatment (Fig. 3A bottom panel, lanes 1 and 2). By contrast, tyrosine-phosphorylated CEACAM1-L was not detected after specific blotting (Fig. 3A top panel, lanes 1 and 2). We have previously demonstrated that SHP-1 interacts with CEACAM1-L

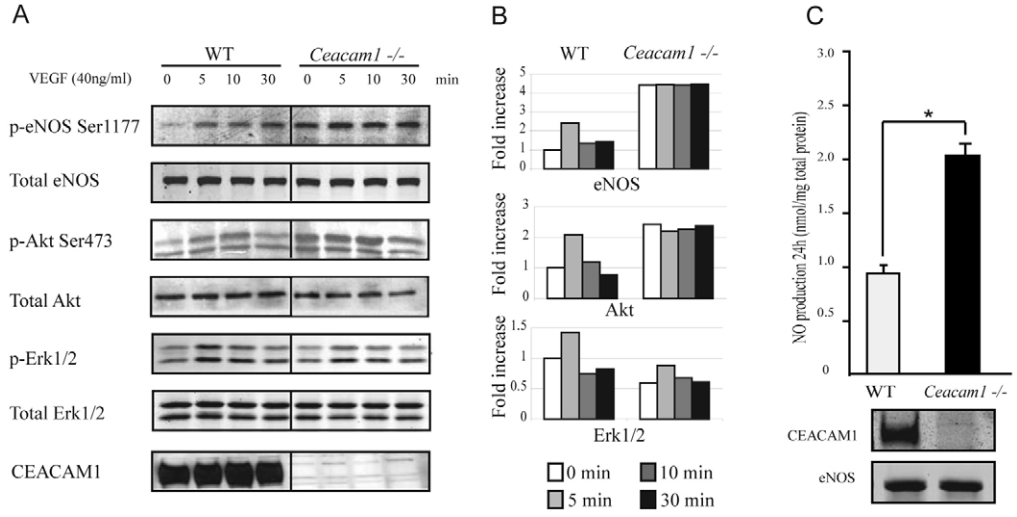


**Fig. 2. VEGFR2-mediated eNOS activation is deficient in *Ceacam1–/–* MLECs.** (**A**) Activation of eNOS, Akt and Erk1/2 using the indicated phosphospecific antibodies was monitored in MLECs stimulated with VEGF (40 ng/ml) for 5, 10 and 30 minutes. CEACAM1 expression levels were also examined using a polyclonal anti-mouse CEACAM1 Ab. (**B**) Quantification of phosphorylated protein and total protein were assessed using the ImageJ software. (**C**) Equal numbers of WT or *Ceacam1–/–* MLECs were plated and grown for 24 hours, whereupon the media was collected and processed for nitrite evaluation. *$P<0.05$.

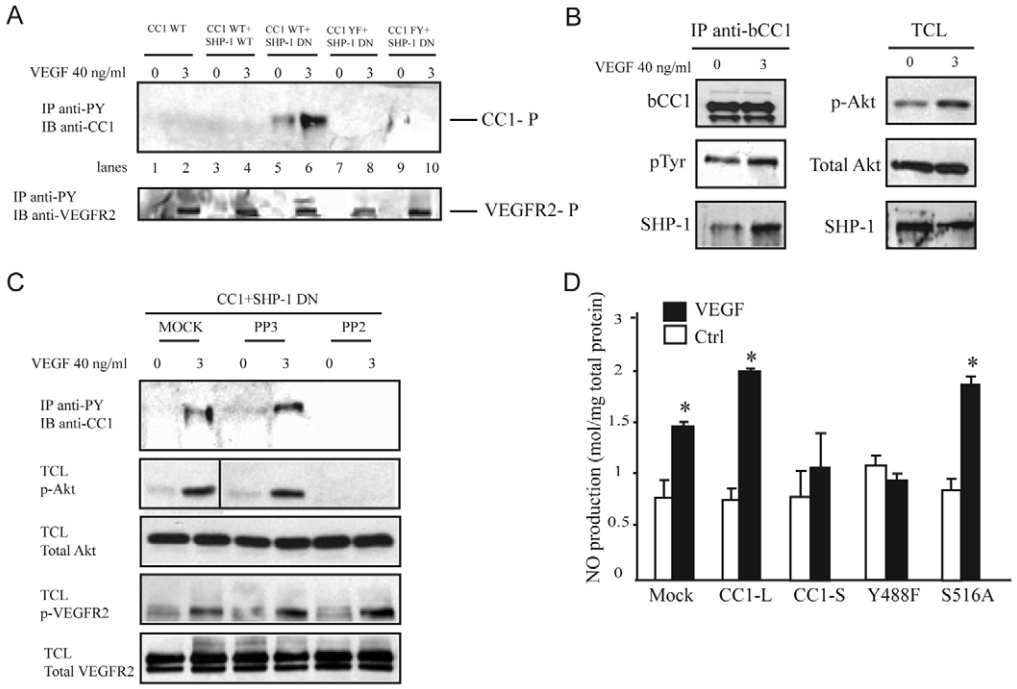


**Fig. 3. CEACAM1 is tyrosine-phosphorylated upon VEGF treatment in a SHP-1- and Src-dependent manner.** (**A**) CEACAM1 is tyrosine-phosphorylated by VEGF in a SHP-1-dependent manner. BAECs were co-transfected with CEACAM1-L (CC1), Tyr515Phe (YF), Tyr488Phe (FY), SHP-1 dominant-negative (DN) or SHP-1 WT as indicated. Cells were stimulated with VEGF (40 ng/ml) for 3 minutes or left untreated. Cell lysates were immunoprecipitated (IP) with an anti-phosphotyrosine (PY) Ab and immunoblotted (IB) using an anti-murine CEACAM1 Ab or VEGFR2 Ab. Equal protein expression was determined by western blotting the total cell lysates (not shown). (**B**) Endogenous bovine CEACAM1 (bCC1) interacts strongly with SHP-1 and is tyrosine-phosphorylated upon VEGF treatment. BAECs were stimulated with VEGF (40 ng/ml) for 3 minutes. CEACAM1 and SHP-1 levels were monitored in endogenous bovine CEACAM1 immunoprecipitates using relevant antibodies. Equal immunoprecipitation levels and Akt activation from BAECs lysates were confirmed by immunoblotting the total cell lysates (TCL). (**C**) Phosphorylation of CEACAM1 occurs via Src-family kinase proteins. BAECs were co-transfected with CEACAM1-L and SHP-1 DN expression vectors. Cells were treated with PP2 or PP3 as indicated (10 μM) for 2 hours and then stimulated with VEGF (40 ng/ml) for 3 minutes. Cell lysates were immunoprecipitated with an anti-phospho-tyrosine Ab and immunoblotted using an anti-murine CEACAM1 Ab. Equal immunoprecipitation levels and Akt and VEGFR2 activation from BAECs lysates were confirmed by immunoblotting the total cell lysates. Phospho-Akt blotting was evaluated from two separate gels. (**D**) Key residues of the ITIM motif of CEACAM1-L are crucial for CEACAM1 phosphorylation and NO production. BAECs were transfected with CEACAM1-L, CEACAM1-S, Tyr488Phe or Ser516Ala as indicated. At 48 hours post-transfection, cell culture medium was processed for the measurement of NO. **P*<0.05 compared with mock-transfected cells.

in colon carcinoma cells (Izzi et al., 1999). We therefore co-transfected WT SHP-1 and CEACAM1-L in BAECs. This approach did not reveal CEACAM1-L tyrosine phosphorylation (Fig. 3A top panel, lanes 3 and 4). We next used a dominant-negative form of SHP-1 (DN-SHP-1) to inactivate the phosphatase. The results demonstrated that coexpression of CEACAM1-L with DN-SHP-1 in BAECs leads to CEACAM1-L tyrosine phosphorylation, but more importantly that its phosphorylation was significantly increased after VEGF treatment (Fig. 3A top panel, lanes 5 and 6). Furthermore, as previously demonstrated in colon carcinoma cells (Izzi et al., 1999), mutation of either CEACAM1-L Tyr515 to Phe (Fig. 3A top panel, lanes 7 and 8) or Tyr488 to Phe (Fig. 3A top panel, lanes 9 and 10) abrogated CEACAM1-L phosphorylation in endothelial cells.

We then verified whether endogenous bovine CEACAM1-L from BAECs interacted with SHP-1 prior to and after VEGF treatment by immunoprecipitation and blotting the immune complexes with an anti-SHP-1 antibody (Fig. 3B). VEGFR2 pathway activation was confirmed by Akt phosphorylation (Fig. 3B, TCL panels). Immunoprecipitation of bovine CEACAM1 revealed three bands at 170, 120, 90 KDa (Fig. 3B, top to bottom, respectively). Furthermore, endogenous bovine CEACAM1-L interacted with SHP-1 in endothelial cells and this interaction increased after VEGF treatment. Moreover, bovine CEACAM1 phosphorylation was slightly increased by 1.5-fold (quantitative data not shown) after VEGF treatment (Fig. 3B, IP panels, 170 KDa band). These data suggest that VEGFR2 activation induces phosphorylation of endogenous bovine CEACAM1-L. This is the first report showing that VEGFR2 activation induces phosphorylation of CEACAM1-L and regulates the association of endothelial CEACAM1-L and SHP-1.

Because CEACAM1-L is phosphorylated by Src-like kinases in epithelial and immune cells (Brummer et al., 1995; Skubitz et al., 1995; Abou-Rjaily et al., 2004; Pantelic et al., 2005; Dubois et al., 2006; Chen et al., 2008; Muller et al., 2009), we looked at whether VEGF-induced CEACAM1-L phosphorylation was elicited by Src kinases in transfected BAECs. To address this, inhibition of Src activity was achieved by pretreating the transfected cells with a specific Src family kinase inhibitor, PP2, before VEGF treatment (Fig. 3C). PP3, the inactive analogue of PP2, was used as a control. Inhibition of Src family kinases by PP2 abrogated Akt phosphorylation after VEGF treatment (Fig. 3C). However, VEGFR2 phosphorylation was not affected by the Src family kinase inhibitor PP2 (Fig. 3C), demonstrating that VEGFR2 is

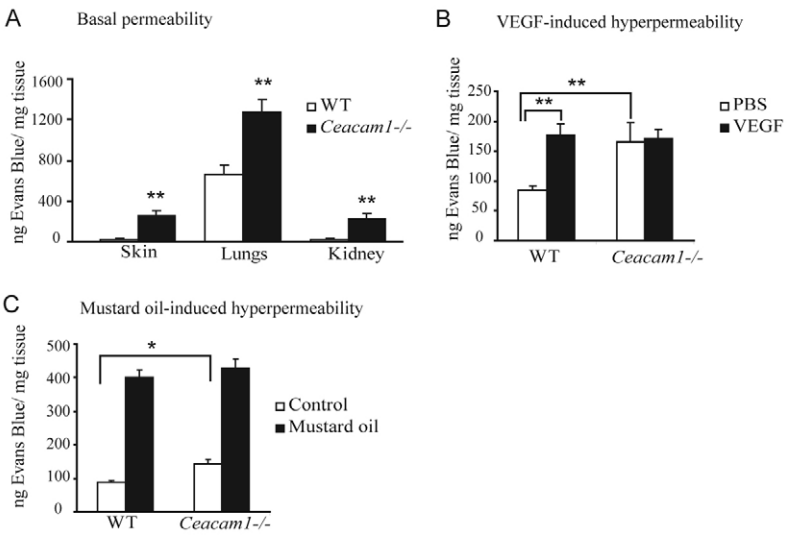


**Fig. 4. Basal permeability is increased and acute VEGF-induced permeability is defective in *Ceacam1–/–* mice.** (**A**) Basal vascular permeability is increased in *Ceacam1–/–* mice. Evans blue dye (50 mg/kg) was injected intravenously and allowed to circulate for 8 hours, at which time the animals were sacrificed and perfused. Evans blue dye was extracted from lungs, kidneys and skin, and measured by absorbance at 620 nm. The results are represented as ng dye/mg tissue ($n$=10). (**B**,**C**) Acute VEGF-elicited permeability is defective in *Ceacam1–/–* mice. At 30 minutes after Evans blue tail vein injection (50 mg/kg), (B) saline or VEGF-A was injected intradermally in the ear (100 ng in 10 µl) or (C) mineral or mustard oil (50 µl of a 15% solution) was topically applied to the dermis for 30 additional minutes. Ears were removed and weighed. The amount of Evans blue dye was measured by absorbance at 620 nm. The results are represented as ng dye/mg tissue weight ($n$=6). *$P$<0.05, **$P$<0.01 compared with WT.

upstream of Src-kinase. Moreover, addition of PP2, but not PP3, to BAECs transfected with CEACAM1-L and DN-SHP1 completely abolished CEACAM1-L tyrosine phosphorylation (Fig. 3C). This result indicates that VEGF-elicited CEACAM1-L phosphorylation in endothelial cells is induced by the Src family kinases.

### Key residues of the ITIM motif of CEACAM1-L are crucial for CEACAM1 phosphorylation and NO production

Previous studies as well as those presented in Fig. 3A revealed that phosphorylation of the key tyrosine residues Tyr488 and Tyr515 within the ITIM motif are required for the function and association of CEACAM1-L with SHP-1 in epithelial and endothelial cells (Huber et al., 1999; Izzi et al., 1999; Dubois et al., 2006; Chen et al., 2008). To evaluate the contribution of these CEACAM1-L key phosphorylation residues in the eNOS signaling pathway, we measured NO release in VEGF-stimulated BAECs transfected with different CEACAM1 mutants (Fig. 3D). Transfection of WT CEACAM1-L slightly increased NO production following VEGF treatment compared with mock-transfected BAECs, confirming the data obtained in the COS-7 reconstituted cells (Fig. 1A). Interestingly, transfection of either CEACAM1-S or the Tyr488Phe CEACAM1-L mutant resulted in lower amounts of released NO from BAECs than from mock-transfected cells (Fig. 3D). However, expression of the CEACAM1-L Ser516Ala mutant did not interfere with NO release, which was as significant as that from cells transfected with WT CEACAM1-L (Fig. 3D). On the basis of these data, CEACAM1-S and the CEACAM1 Tyr488Phe mutant might constitute dominant-negative mutants in the VEGF-mediated activation of eNOS. Moreover, blotting with specific phospho-eNOS Ser1177 antibody revealed that eNOS is correctly activated after VEGF treatment (supplementary material Fig. S3). This result demonstrates that although both CEACAM1-S and Tyr488Phe might act as dominant negative with regards to NO production after VEGF treatment (Fig. 3D), Ser 1177 eNOS phosphorylation is not affected. Overall, these results confirm the involvement of the CEACAM1 long cytoplasmic domain and more precisely of the Tyr488 residue in VEGF-dependent eNOS activation and NO release from endothelial cells.

### Basal permeability is increased and acute VEGF-induced permeability is defective in *Ceacam1–/–* mice

Our previous results suggested that CEACAM1 deletion produced vascular leakage upon induction of neo-vascularization, implying that CEACAM1 participates in the regulation of vascular integrity and permeability of newly formed vessels (Horst et al., 2006). In turn, the data presented here demonstrates that eNOS activity, a key mediator of VEGF-induced vascular permeability, is regulated by CEACAM1-L. We therefore questioned whether basal vascular permeability and acute VEGF-elicited vascular permeability were both dependent on CEACAM1.

To assess basal vascular permeability, we quantified Evans blue dye extravasation from the lungs, skin and kidney tissues at 8 hours post-administration. We observed significantly increased extravasation of Evans blue dye in *Ceacam1–/–* mouse organs as compared with those of the WT control mice (Fig. 4A). Thus, CEACAM1 deletion induces increased basal vascular permeability. To assess VEGF-elicited acute vascular permeability, a modified Miles assay was performed following intradermal injection of VEGF in the ear (Fig. 4B). Spectrophotometric analyses were performed on dissected ears 30 minutes after VEGF injection. VEGF robustly induced vascular permeability in the skin of WT mice, as shown by increased leakage of Evans blue dye (Fig. 4B). However, in *Ceacam1–/–* mice, extravasation of Evans blue dye was already strongly increased at basal level (Fig. 4A) such that VEGF treatment did not induce any further increase in permeability (Fig. 4B). We next investigated vascular leakage in ear skin in response to mustard oil, an inflammatory agent that stimulates acute plasma leakage in the skin (Fig. 4C). Mice were injected intravenously with Evans blue dye, followed by topical application of mustard oil to the epidermis of the ear. The results showed that mustard oil treatment provoked an equivalent increase in dye leakage in the vessels of both WT and *Ceacam1–/–* mice, demonstrating that the permeability effect responds specifically to VEGF. Taken together, these data indicate that CEACAM1 deletion induces increased basal vascular permeability and that *Ceacam1–/–* mice suffer from a VEGF-elicited acute permeability defect.

### Vascular ultrastructure is disrupted in *Ceacam1–/–* mice

To determine whether this increased basal vascular permeability and the acute vascular permeability defect in *Ceacam1–/–* mice

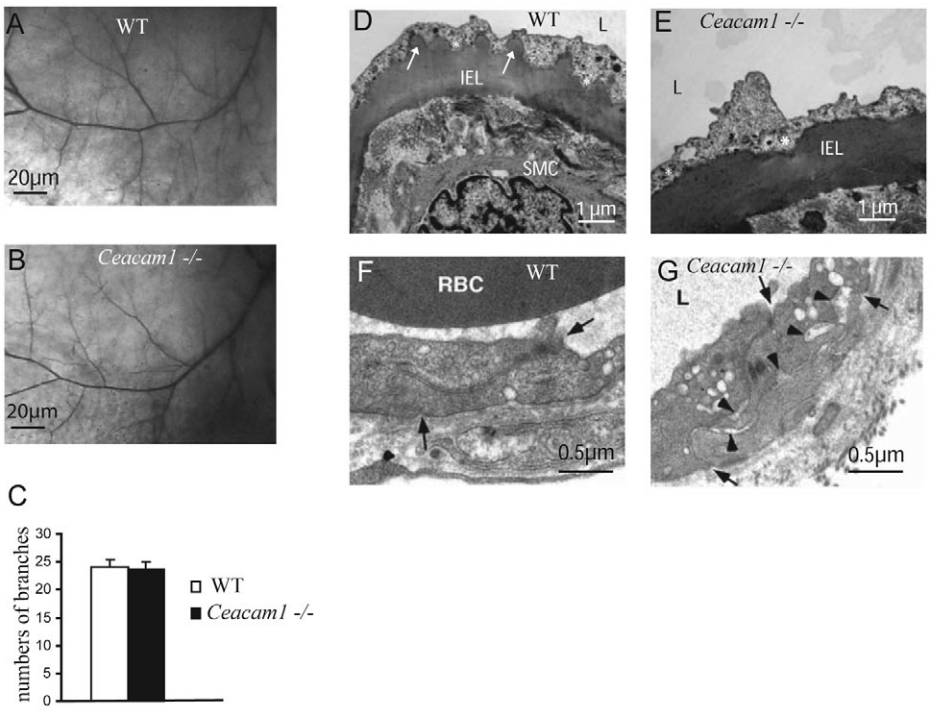


**Fig. 5. Vascular ultrastructure is disrupted in *Ceacam1–/–* mice.** (**A–C**) Normal vasculature is seen in the flank skin of (A) WT and (B) *Ceacam1–/–* mice ($n$=3 for each). (C) Quantification showed no differences in the number of branches per area between genotypes. Results are expressed as mean + s.d. (**D–G**) Electron microscopy on aorta (D,E) and dermal vasculature (F,G). In WT mice (D), ECs lining the lumen of aorta are intimately associated with the internal elastic lamina (IEL) with only a small subendothelial space (marked by an asterisk). Numerous projections of the IEL (white arrows) closely interdigitate with the EC surface. By contrast, the border of the IEL underlying the ECs in the *Ceacam1–/–* aorta (E) is smooth and does not contain interdigitating projections of elastic lamina as seen in WT aorta. In some areas, the subendothelial space appears to be widened. In the dermis, EC junctions in dermal microvessels in WT mice (F) are tight and uniform in appearance, whereas those in the *Ceacam1–/–* skin (G) are irregular with dilated regions (arrowheads) that are often connected to numerous transcytotic vesicles. Black arrows in F and G indicate the beginnings and ends of the junctions. SMC, smooth muscle cell; L, lumen; RBC, red blood cell.

was influenced by vascular structural abnormalities, we investigated the organization of the dermal vasculature (Fig. 5A,B). No differences in the overall vessel patterns were observed between *Ceacam1–/–* and WT mice nor the in degree of branching, based on the fact that the number of branching points per area was similar between the two genotypes (Fig. 5C). To investigate the ultrastructure of blood vessels in more detail, the aorta and the microvasculature of the skin were examined by electron microscopy (Fig. 5D–G). In the aorta, contacts between the endothelial cells and the internal elastic lamina (IEL) were altered (Fig. 5D,E). More precisely, projections of the IEL that normally interdigitate with the adlumenal surface of the endothelial cells were not present or were flattened in the *Ceacam1–/–* mice, thus leaving a gap between the cells and IEL (Fig. 5E). We next investigated the ultrastructure of the dermal microvessels (Fig. 5F,G). In contrast to the tight, uniform junctions seen between endothelial cells in WT mice, cells in the *Ceacam1–/–* dermis showed looser and more irregular connections. Additionally, transcytotic vesicles were often seen fused with the junctions in the *Ceacam1–/–* mice, but only rarely so in the WT vessels (Fig. 5F,G). Taken together, these data demonstrate that there are obvious vascular abnormalities in the *Ceacam1–/–* mice that likely contribute to the vascular permeability defects seen in these animals.

### CEACAM1-deficient mice exhibit increased chronic vascular tumor permeability

Finally, in light of the vascular permeability characteristics of the *Ceacam1–/–* normal vessels, we examined whether this phenotype can also be extended in a pathological model, such as in a tumor environment. To address this, Lewis lung carcinoma (LLC) cells were injected into the dorsal flank of 6- to 8-week-old WT and *Ceacam1–/–* mice. We first examined tumor burden by monitoring tumor growth. As seen in Fig. 6A, LLC cells implanted in *Ceacam1–/–* mice grew significantly faster than in WT mice. To assess tumor permeability, Evans blue dye was injected intravenously when tumor sizes reached 500–1000 $mm^3$ as measured with calipers. Following perfusion with saline, the dye was extracted from each tumor as described in Materials and Methods, and quantified spectrophotometrically (Fig. 6B). Tumors grown in *Ceacam1–/–* mice had significantly higher extravasation of Evans blue dye than WT mice, corresponding to increased permeability of the tumor vasculature. Moreover, 10 days post-injection, tumors implanted into *Ceacam1–/–* mice exhibited a higher density of endothelial CD31-positive structures than tumors implanted into WT mice (Fig. 6C). We also examined tumor vessel maturity by quantifying smooth muscle actin (SMA)-positive cells. We found that recruitment of α-SMA-positive mural cells was impeded in tumors growing in *Ceacam1–/–* mice (Fig. 6C). Overall, these data suggest that CEACAM1 deletion provokes increased tumor proliferation and increased tumor density of immature blood vessels, which results in increased tumor vascular permeability.

## Discussion

In this article, we define a novel role for the CEACAM1 glycoprotein as a key regulator of VEGFR2-mediated angiogenesis and vascular permeability in vitro and in vivo. Many angiogenic factors use NO as a mediator of their vascular functions. VEGF treatment of ECs increases NO production, Akt and eNOS phosphorylation and, consequently, eNOS activity (Sessa, 2004). Akt1 expression and activity are required for pathological angiogenesis in a hindlimb ischemia model or in response to VEGF-induced acute permeability (Ackah et al., 2005). Moreover, eNOS-derived NO plays a crucial role in acute inflammation, in particular by affecting early changes in vascular permeability (Cirino et al., 2003). The role played by CEACAM1 in endothelia signal transduction has so far remained ill-defined. Our work represents the first report, to our knowledge, of a functional link between CEACAM1 and the eNOS/Akt permeability pathway.

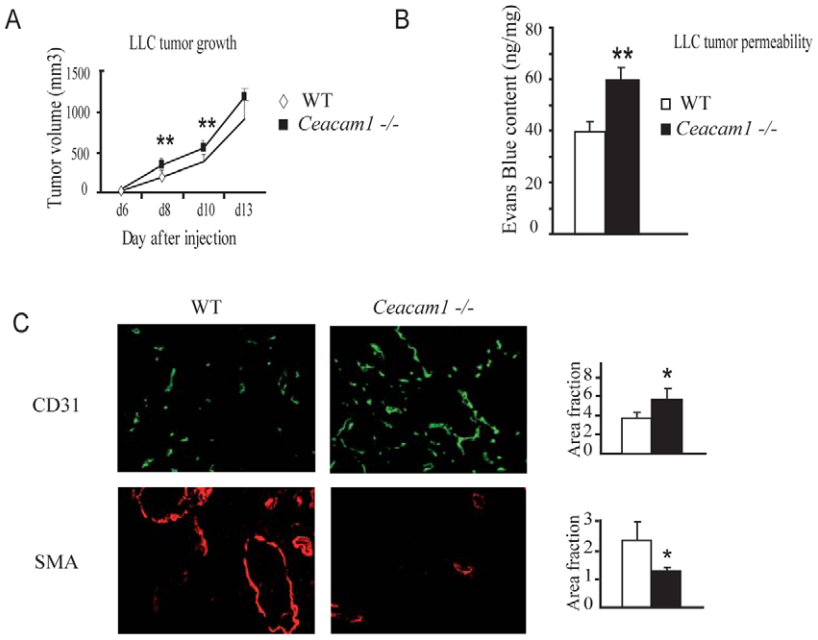


**Fig. 6. Permeability of tumor vasculature is increased in *Ceacam1–/–* mice.** $1\times10^6$ LLC cells were injected subcutaneously into the left flank of 8-week-old WT and *Ceacam1–/–* mice (*n*=7). (**A**) LLC implanted in *Ceacam1–/–* mice grew faster than in WT mice. Tumors were allowed to grow for 14 days and tumor volumes were assessed after measuring with calipers every 2 days. (**B**) Tumor vascular permeability is increased in *Ceacam1–/–* mice. Tumor permeability was evaluated after tail vein injection of Evans blue dye (50 mg/kg) when tumor size reached 500–1000 $mm^3$. Mice were perfused 30 minutes after dye injection for 1 minute with saline. Tumors were excised and weighed before Evans blue dye extraction in formamide at 56°C for 48 hours. The amount of extracted Evans blue dye was normalized to ng/mg tumor weight. (**C**) LLC implanted in *Ceacam1–/–* mice showed increased vascular density staining (CD31) but decreased mature vessel staining (SMA). Immunohistochemistry was performed on frozen tumor tissue according to standard procedures. Sections were incubated with primary antibodies to CD31 and SMA, followed by incubation with secondary Alexa-Fluor-labeled antibodies (left panels). Quantitative analyses of immunostained images captured from six to eight fields per tumor section (*n*=7) were assessed using ImageJ software (right). **P*<0.05, ***P*<0.01 compared with WT.

We demonstrate here that in an endogenous endothelial cell model (MLEC cells), CEACAM1 deletion causes aberrant basal phosphorylation of both Akt and eNOS, leading to an absence of NO production upon VEGF treatment. On the other hand, expression of CEACAM1-L contributes to eNOS activity in a reconstituted system (COS-7). This result can be explained by the fact that COS-7 cells do not express either eNOS or VEGFR2 and that co-transfection of both eNOS and VEGFR2 need to be performed for evaluation of eNOS-dependent NO production upon VEGF treatment. Whereas the reconstituted system was powerful in evaluating the impact of CEACAM1 on the eNOS activity and demonstrated that CEACAM1 is a potent regulator of eNOS activity, the endogenous endothelial cell model allowed us to define the mechanism by which CEACAM1 interferes with eNOS activity.

Systemic deletion of CEACAM1 leads to increased in vivo basal vascular permeability in the lungs, skin and kidneys. Miles assays performed in *Ceacam1–/–* mice revealed that basal vascular permeability was increased in ear skin and was not further enhanced by VEGF treatment. Taken together, these data suggest that the in vivo increased basal vascular permeability due to the absence of CEACAM1 correlates with the in vitro increased basal Akt and eNOS phosphorylation.

VEGF-induced acute vascular permeability defects observed in *Ceacam1–/–* mice are consistent with a deficiency in VEGF-induced eNOS activation and, consequently, with the deficiency in NO production observed in MLECs. We measured NO accumulation in both WT and *Ceacam1–/–* MLECs after culturing them for 24 hours. Our results showed that NO accumulation is significantly higher in *Ceacam1–/–* MLECs than in the WT MLECs, which is consistent with an elevated basal phosphorylation level of eNOS proteins before stimulation. One possible explanation is that, in *Ceacam1–/–* mice, eNOS is constantly in the hyperphosphorylated state, which leads to higher production of NO, as observed after a 24-hour accumulation period. However, in order to induce VEGF-stimulated NO production, eNOS needs to revert back to a non-phosphorylated state. Because eNOS is already hyperphosphorylated, a 30-minute VEGF treatment results in a completely deficient NO induction in *Ceacam1–/–* MLECs.

In addition, Akt is an essential molecule for insulin-mediated production of endothelial NO; cells expressing a mutant form of eNOS with a disrupted Akt phosphorylation site are unable to produce NO in response to insulin (Montagnani et al., 2001). It has also been demonstrated that insulin resistance and hyperinsulinemia induce endothelial dysfunction, possibility due to insufficient activation of eNOS, with a subsequent absolute decrease of NO bioavailability (Potenza et al., 2009). We and others have shown that C*eacam1–/–* mice suffer from hepatic insulin resistance and are thus predisposed to liver steatosis and liver damage (Lee et al., 2008; Xu et al., 2009). Consequently, CEACAM1-mediated insulin clearance and acute vascular permeability deficiencies are probably directly interrelated through absence of eNOS-dependent NO production in *Ceacam1–/–* mice.

Because CEACAM1-L is phosphorylated in activated T cells and upon both EGFR and insulin receptor activation in epithelial cells, we next questioned whether CEACAM1-L was phosphorylated in response to VEGF in endothelial cells. We have previously shown that tyrosine phosphorylation of the CEACAM1-L cytoplasmic domain in CT51 mouse colonic carcinoma cells led to its binding to the protein tyrosine-phosphatase SHP-1 and that this event required the presence of both Tyr488 and Tyr515 within the ITIM motif (Huber et al., 1999; Izzi et al., 1999). Indeed, CEACAM1-L is dephosphorylated by SHP-1 in epithelial and lymphocytic cells (Dubois et al., 2006; Nagaishi et al., 2006; Lobo et al., 2009). In colon carcinoma, the ability of CEACAM1-L to inhibit in vivo tumor development depends on its interaction with SHP-1 (Izzi et al., 1999). In hepatocytes, CEACAM1 is a substrate of SHP-1 and modulates metabolic homeostasis and hepatic insulin clearance (Dubois et al., 2006). Furthermore, CEACAM1 acts as an inhibitory TCR co-receptor in T lymphocytes, a function that depends on the presence of SHP-1 and the ITIM motifs of CEACAM1 (Nagaishi et al., 2006). Here, we demonstrate that CEACAM1-L tyrosine phosphorylation in ECs on both Tyr488

and Tyr515 residues is detectable after VEGF treatment in a SHP-1-dependent manner, as this phosphorylation is only detectable when SHP-1 is inactivated by a dominant-negative form. We have also shown that endogenously tyrosine-phosphorylated bovine CEACAM1-L binds to bovine SHP-1 upon VEGF treatment of BAECs, which confirms the link between CEACAM1 function and its association with SHP-1. Thus, similar to its function in T cells, colon carcinoma and hepatocytes, CEACAM1 might act as a regulatory VEGFR2 co-receptor, through its recruitment of SHP-1.

Although there is now a clear link between CEACAM1 and SHP-1, less is known about the function of SHP-1 in the VEGF signaling pathway. Two studies demonstrated that tyrosine Tyr951/996 and Tyr1054/1059 within the dimeric complex of VEGFR2 are dephosphorylation targets for SHP-1 and SHP-2, which negatively control VEGFR2 activity (Kroll and Waltenberger, 1997; Bhattacharya et al., 2008). Other reports implicate SHP-1 in mediating inactivation of VEGFR2 (Nakagami et al., 2002; Seo et al., 2003). Further studies will be required to determine the mechanisms by which CEACAM1 interferes with SHP-1 and VEGFR2 activity in endothelial cells. One possibility is that SHP-1 is recruited to CEACAM1-L after VEGFR2 activation to dephosphorylate CEACAM1-L, but that it does not directly target VEGR2, eNOS or Akt.

Furthermore, using PP2 as a specific Src family kinase inhibitor, we showed that tyrosine-phosphorylation of CEACAM1-L by VEGF in ECs is dependent upon Src family kinase activity. This is consistent with previous observations that the tyrosines within the CEACAM1-L ITIMs are phosphorylated by c-Src kinase in epithelial cells, Lck kinase in T cells, Btk kinase in B cells, Lyn in neutrophils, and insulin receptor as well as epidermal growth factor receptor tyrosine kinases in hepatocytes (Brummer et al., 1995; Skubitz et al., 1995; Abou-Rjaily et al., 2004; Pantelic et al., 2005; Dubois et al., 2006; Chen et al., 2008; Muller et al., 2009). We have previously shown in a mouse colon tumor model that CEACAM1-L acts as a tumor growth inhibitor. Notably, a single CEACAM1-L mutation of Tyr488 was sufficient to reverse the inhibition of in vivo tumor growth. Here, expression of Tyr488Phe CEACAM1-L mutant resulted in lower amounts of released NO from BAECs than that from mock-transfected cells, thus demonstrating the contribution of the CEACAM1-L Tyr488 residue to the eNOS signaling pathway. These data represent the first report of a functional link between CEACAM1-L and the VEGFR2/eNOS pathways.

VEGF stimulation of endothelial cells activates at least two signaling pathways that converge toward NO production. VEGF stimulates intracellular calcium mobilization in endothelial cells through the activation of phospholipase C-γ (PLCγ) (He et al., 1999). Simultaneously, the PI3K-dependent activation of Akt by VEGFR2 is responsible for eNOS phosphorylation on Ser1176 (1177 in human eNOS), which leads to increased eNOS activity and NO release (Fulton et al., 1999). We clearly demonstrate here that VEGF-induced phosphorylation of Ser1177 of eNOS is affected by CEACAM1 deletion. Further studies will need to address whether $Ca^{2+}$ signaling and PLCγ activation upon VEGF stimulation is regulated by CEACAM1. However, our results identify eNOS phosphorylation on Ser1176 by Akt as an obligatory event for eNOS activation and NO production in response to VEGF, and suggest that other VEGF signaling pathways (such as PLCγ activation) are not primary events for eNOS activation (Blanes et al., 2007).

Normal vasculogenesis does not appear to be deficient in the *Ceacam1–/–* mice because no obvious defects were observed in the overall vascular structure either during embryogenesis or in adult tissues. In fact, vascular trees exhibited the same number of branches and similar blood vessel size in WT and *Ceacam1–/–* mice. However, electron microscopy analyses detected abnormalities in the subendothelial region in the aorta and in the dermal microvascular ultrastructure in *Ceacam1*-null mice. The intima of blood vessels consists of an EC layer on the underlying IEL. Developmental defects in the IEL in human arteries might cause EC disruption and thereby initiate the process of intimal thickening (Jones et al., 2005). Abundant literature has focused on the EC layer as a barrier to macromolecular entry; however, recent studies have suggested that IEL permeability is not static and could contribute to pathological changes in the artery wall (Lee et al., 2005). Our results show a gap in the contact zone between the ECs and the IEL in the *Ceacam1–/–* aorta. Moreover, the dermal vascular ultrastructure was also affected in these animals, suggesting a generalized defect in vascular integrity. These data provide evidence that CEACAM1 deletion results in vascular ultrastructural dysfunction, which might cause the increased basal vascular permeability observed in *Ceacam1–/–* animals.

Finally, to evaluate the impact of CEACAM1 deletion in chronic vascular permeability, we used a Lewis lung carcinoma tumor model and showed that tumors developing in *Ceacam1–/–* mice displayed increased vascularization but produced fewer mature blood vessels. Moreover, tumor vascular permeability was significantly increased in *Ceacam1–/–* mice. Although vascular leakage is not a prerequisite for blood vessel growth, increased vascular permeability often coincides with the early stages of angiogenesis, particularly in solid tumors (Fukumura et al., 1997). Thus, our results suggest that perturbation of CEACAM1 expression keeps the newly formed vessels structurally unstable, as evidenced by our findings showing the reduced assembly of α-SMA-positive mural cells to the wall of tumor vessels grown in *Ceacam1–/–* mice. ECs of such unstable vessels are more sensitive to VEGF, which might explain the increased vascularization and, consequently, the increased tumor growth in *Ceacam1–/–* mice. It has been reported that endothelial CEACAM1 overexpression results in a significant increase in expression of angiopoietin-1, which acts as a ligand of the Tie-2 receptor and serves as the major system for stabilization of new vessels (Thurston et al., 1999; Kilic et al., 2005). Moreover, the ‘vasculogenic zone’ residing in the wall of adult human blood vessels has been shown to serve as a source of progenitor cells for postnatal vasculogenesis and thus contributes to tumor vascularization (Zengin et al., 2006). Indeed, new vessels formed by these vascular wall-resident endothelial progenitor cells express markers for angiogenically activated endothelial cells, such as CEACAM1 (Zengin et al., 2006). This reveals that the ability of tumors to attract and develop a mature vasculature depends on the presence of CEACAM1.

To conclude, our study reveals that CEACAM1 is involved in cross-talk with VEGFR2, a function that is consequently regulated by Src-mediated tyrosine phosphorylation and SHP-1-elicited dephosphorylation. CEACAM1 therefore appears to act as a vascular guard in endothelial cells. Its expression contributes to coordination of the endothelial permeability responses in normal cells, whereas it absence weakens this barrier and allows increased development of an immature vascular network and augmented tumor growth in pathological situations.

## Materials and Methods

### Cell culture

Generation of *Ceacam1*–/– mice has previously been described (Leung et al., 2006). Microvascular MLECs were isolated from lungs of 2–3 month old WT and *Ceacam1*–/– mice as described previously (Horst et al., 2006) and grown in DMEM:F12 (1:1) medium (Gibco), containing 20% FBS (Hyclone), 0.05 mg/ml endothelial mitogen (Biomedical Technologies), 0.05 mg/ml heparin (Sigma), 100 U/ml penicillin and 100 μg/ml streptomycin (Multicell). BAECs (Vec Technologies) and COS-7 cells were grown in DMEM medium, supplemented with 100 U/ml penicillin, 100 μg/ml streptomycin and 10% FBS.

### Protein detection, immunoblotting and immunoprecipitation

Cells were lysed in lysis buffer containing 100 mM TrisCl (pH 8.0), 0.1 mM EDTA, 0.1 mM EGTA, 150 mM NaCl, 1% Triton X-100, 20 mM NaF, 1 mM $Na_3VO_4$, 1 mM $NaH_2PO_4$ and complete EDTA-free Protease Inhibitor cocktail (Roche). Protein concentrations were determined using a BCA Protein Assay Kit (Pierce ThermoScientific). Equal amounts of proteins were separated on 8% SDS-PAGE gels, transferred to PVDF membranes and immunoblotted with the following antibodies: anti-phosphoSer1177 eNOS Ab, anti-eNOS Ab, anti-phosphoSer473 Ab Akt, anti-pan Akt Ab, anti-phosphoErk1/2 Ab, anti-Erk1/2 Ab or anti-CEACAM1 Ab 3759, anti-phosphoTyr1175 VEGFR2 Ab, anti-pan VEGR2 Ab (all from Cell Signaling, except CEACAM1 Ab, custom made rabbit polyclonal). Detection was done using the Western Lightning Plus-ECL kit (Perkin-Elmer). For immunoprecipitations, BAECs were solubilized with lysis buffer (see above). Soluble proteins (1 mg) were pre-cleared with 10 μg mouse IgG (Jackson Laboratories) and Protein G-Sepharose (50 μl of a 50% slurry; Invitrogen) for 1 hour each at 4°C, and then incubated with murine anti-bovine CEACAM1 antibody AH-13A5-C1 (10 μg) or anti-phosphotyrosine (4G10) antibody (10 μg) at 4°C for 18 hours. The immune complexes were incubated with Protein G-Sepharose for an additional 1 hour and collected by centrifugation, washed with lysis buffer, boiled in SDS sample buffer, separated by SDS-PAGE, transferred onto a PVDF membrane and immunoblotted with various Abs (bovine CEACAM1 antibody AH-13A5-C1, anti-phosphotyrosine 4G10 and anti-SHP-1 rabbit polyclonal antibody 838) (Beauchemin et al., 1997). CECAM1-L immunoprecipitation from MLECs was achieved with a rabbit anti-L domain antibody (Ab 836) (Beauchemin et al., 1997). Transfections were performed in COS-7 cells and BAECs using Lipofectamine 2000 according to manufacturer's protocol (Invitrogen). Immunoprecipitation and western blot analyses were performed 48 hours after transfections. cDNAs coding for bovine eNOS (in pcDNA3), human VEGFR-2 (in pRK7), mouse CEACAM1-S, CEACAM1-L, Tyr488Phe, Tyr515Phe and Ser516Ala (in pXM139) were described previously (Huber et al., 1999; Duval et al., 2007).

### Nitric oxide release analysis

Cell media was processed for the measurement of nitrite ($NO_2^-$), the stable breakdown product of NO in aqueous solution, by NO-specific chemiluminescence using a NO analyzer (NOA 280i, GE Ionics Instruments) (Sessa et al., 1995). VEGF-A (40 ng/ml)-stimulated NO production from MLECs was measured on serum-starved cell media (6 hours), after removing proteins by ethanol precipitation. The media was processed for measurement of nitrite levels 30 minutes following cell stimulation. Media was also collected from WT and *Ceacam1*–/– MLECs after culturing them for 24 hours and was evaluated for nitrite production. Transfected COS-7 cells and BAECs were processed for the measurement of nitrite as described above, at 48 hours after transfections.

### siRNA-mediated silencing of bovine CEACAM1

siRNA duplexes designed to target bovine CEACAM1 were synthesized by Sigma as follows: for siRNA1, 5′-CCCAGAACACCUCCUACAU-3′ (sense) and 5′-AUGUAGGAGGUGUUCUGGG-3′ (antisense); for siRNA2, 5′-CCCUAUGUGUGCGAAGCCU-3′ (sense) and 5′-AGGCUUCGCACACAUAGGG-3′ (antisense), for siRNA3, 5′-CAUUCACCCUGAAUGUCCU-3′ (sense) and 5′-AGGACAUUCAGGGUGAAUG-3′ (antisense); and for Scramble, 5′-CUUGCUUAAUGAACAUAUA-3′ (sense) and 5′-UAUAUGUUCAUUAAGCAAG-3′ (antisense). BAEC cells were transfected using Lipofectamine 2000 reagent (Invitrogen) with 100 pmol siRNAs. After 48 hours, BAECs were treated with VEGF and processed for the measurement of nitrite as described above.

### Miles acute and basal vascular permeability assays

To measure acute permeability, Evans blue dye (50 mg/kg body weight) was injected intravenously into the tail vein of C57Bl/6 WT and *Ceacam1*–/– mice ($n$=10 for each genotype) prior to intradermal injection of a 10 μl (100 ng) of VEGF-A (National Cancer Institute) or to topical ear application of 50 μl of 15% mustard oil (Allyl isothiocyanate, Sigma). As controls, we used either PBS or mineral oil. The mice were sacrificed 30 minutes later and the ears removed and weighed. For quantitative measurement of extravasated Evans blue dye, tissues were placed in 500 μl formamide and incubated at 56°C for 48 hours. The amount of extracted Evans blue dye was determined by measuring the absorbance at 620 nm and calculating against a standard curve of known Evans blue dye concentrations. To measure basal vascular permeability, mice were perfused for 8 hours after Evans blue injection. Lungs, kidney and skin were dried for 20 hours at 65°C and the extravasated Evans blue dye quantified in dried organs as described above. Data is presented as nanograms dye per milligram tissue.

### Analysis of dermal vasculature

WT and *Ceacam1*–/– mice were used for the quantification of branches extending from the long thoracic artery. A central incision was made on the ventral surface of the animal, and the skin opened laterally to expose the posterior surface of the skin. Images were taken of the long thoracic artery using a Nikon camera.

### Electron microscopy

Aortic wall segments of three WT and three *Ceacam1*–/– mice were fixed in 4.5% glutaraldehyde for 18 hours at 4°C, then stained en bloc with 1% osmium tetroxide in 0.1 M sodium cacodylate buffer (pH 7.4) at 4°C for 90 minutes. After extensive washes, 1% uranyl acetate was applied in 70% ethanol. Tissues were then dehydrated followed by Epon embedding. Blocks were polymerized at 60°C for 2 days and then 80 nm sections were cut on a Reichert-Jung Ultracut ultramicrotome. Sections were stained with 1% uranyl acetate in distilled water followed by 0.4% lead citrate for 5 minutes to enhance contrast. Images were captured on a Zeiss transmission electron microscope (EM 902A) at 80 kV. Digital image acquisition was performed on a MegaViewII slow-scan-CCD camera connected to a PC running ITEM 5.0 software (Soft-imaging-systems, Münster, Germany). For skin tissue, samples were treated en bloc with osmium tetroxide, tannic acid and uranyl acetate, then dehydrated and embedded in Epon as previously described (Davis, 1993). Thin (60 nm) sections were counterstained with methanolic uranyl acetate and lead citrate, and digital images obtained using a Tecnai 12 transmission electron microscope at 120 kV.

### Tumor development and tumor permeability assays

LLC (Lewis lung carcinoma, ATCC) cells were grown in DMEM medium supplemented with 10% FBS (Gibco). The cells were grown to 80% confluency and $1\times10^6$ LLC cells were injected subcutaneously in the left flank of 8-week-old WT and *Ceacam1*–/– mice ($n$=7 for each genotype). Tumors developed for 14 days. Tumor size was measured every 2 days with calipers to assess tumor volume (length×height×width×0.5236). For tumor permeability assays, Evans blue dye (50 mg/kg) was injected intravenously in the tail vein when tumor sizes reached 500–1000 $mm^3$. Mice were subjected to 1 minute of saline perfusion 30 minutes after dye injection. Tumors were then excised, weighed and Evans blue dye was extracted in 1 ml formamide at 56°C for 48 hours. The extracted dye was normalized to nanograms dye per milligram tumor weight. Immunohistochemistry was performed on frozen tumor tissue according to standard procedures. Briefly, after acetone fixation, sections were incubated with primary antibodies to CD31 (1:600; Pharmingen) and SMA (1:800; Sigma) followed by incubation with secondary antibodies (1:2000, Alexa Fluor; Invitrogen). Quantitative analysis of images captured from 6–8 fields per tumor section was assessed using NIH ImageJ software (http://rsbweb.nih.gov/ij/).

### Statistical analyses

Data are presented as means + s.e.m. unless indicated otherwise. Statistical comparisons between groups were performed using one- or two-way analysis of variance (ANOVA) with repeated measures followed by Tukey's or Bonferroni's post-hoc $t$-test, respectively, as appropriate. $P$ values <0.05 were considered statistically significant.

We wish to thank Janusz Rak for his helpful corrections and comments on the manuscript and Christophe Langlois for technical help. This work was supported by grants from the Canadian Institutes for Health Research (N.B. and J.-P.G.). A.-L.N. and S.L. were respectively recipients of either a post-doctoral fellowship from the Fonds de la Recherche en Santé du Québec (FRSQ) or a studentship from the Canadian Institutes of Health Research. E.C.D. is a Canada Research Chair and was supported by a Canadian Institutes of Health grant (MOP86713). The funders had no role in study design, data collection and analysis, decision to publish, or preparation of the manuscript. A.-L.N. performed and designed research experiments, analyzed the data and wrote the manuscript. S.L., M.O., H.J., E.C.D., V.B., C.T. contributed data. R.K. provided antibodies. S.E., J.-P.G. and N.B. designed research experiments, analyzed data and wrote the manuscript. The authors have no conflicts of interest to declare.

Supplementary material available online at
http://jcs.biologists.org/cgi/content/full/123/24/4221/DC1

## References

**Abou-Rjaily, G. A., Lee, S. J., May, D., Al-Share, Q. Y., Deangelis, A. M., Ruch, R. J., Neumaier, M., Kalthoff, H., Lin, S. H. and Najjar, S. M.** (2004). CEACAM1 modulates epidermal growth factor receptor-mediated cell proliferation. *J. Clin. Invest.* **114**, 944-952.

**Ackah, E., Yu, J., Zoellner, S., Iwakiri, Y., Skurk, C., Shibata, R., Ouchi, N., Easton, R. M., Galasso, G., Birnbaum, M. J. et al.** (2005). Akt1/protein kinase Balpha is critical for ischemic and VEGF-mediated angiogenesis. *J. Clin. Invest.* **115**, 2119-2127.

**Beauchemin, N., Kunath, T., Robitaille, J., Chow, B., Turbide, C., Daniels, E. and Veillette, A.** (1997). Association of biliary glycoprotein with protein tyrosine phosphatase SHP-1 in malignant colon epithelial cells. *Oncogene* **14**, 783-790.

**Bhattacharya, R., Kwon, J., Wang, E., Mukherjee, P. and Mukhopadhyay, D.** (2008). Src homology 2 (SH2) domain containing protein tyrosine phosphatase-1 (SHP-1) dephosphorylates VEGF Receptor-2 and attenuates endothelial DNA synthesis, but not migration*. *J. Mol. Signal.* **3**, 8.

**Blanes, M. G., Oubaha, M., Rautureau, Y. and Gratton, J. P.** (2007). Phosphorylation of tyrosine 801 of vascular endothelial growth factor receptor-2 is necessary for Akt-dependent endothelial nitric-oxide synthase activation and nitric oxide release from endothelial cells. *J. Biol. Chem.* **282**, 10660-10669.

**Brummer, J., Neumaier, M., Gopfert, C. and Wagener, C.** (1995). Association of pp60c-src with biliary glycoprotein (CD66a), an adhesion molecule of the carcinoembryonic antigen family downregulated in colorectal carcinomas. *Oncogene* **11**, 1649-1655.

**Carmeliet, P.** (2003). Angiogenesis in health and disease. *Nat. Med.* **9**, 653-660.

**Chen, Z., Chen, L., Qiao, S. W., Nagaishi, T. and Blumberg, R. S.** (2008). Carcinoembryonic antigen-related cell adhesion molecule 1 inhibits proximal TCR signaling by targeting ZAP-70. *J. Immunol.* **180**, 6085-6093.

**Cirino, G., Fiorucci, S. and Sessa, W. C.** (2003). Endothelial nitric oxide synthase: the Cinderella of inflammation? *Trends Pharmacol. Sci.* **24**, 91-95.

**Davis, E. C.** (1993). Smooth muscle cell to elastic lamina connections in developing mouse aorta. Role in aortic medial organization. *Lab. Invest.* **68**, 89-99.

**Dubois, M. J., Bergeron, S., Kim, H. J., Dombrowski, L., Perreault, M., Fournes, B., Faure, R., Olivier, M., Beauchemin, N., Shulman, G. I. et al.** (2006). The SHP-1 protein tyrosine phosphatase negatively modulates glucose homeostasis. *Nat. Med.* **12**, 549-556.

**Duval, M., Le Boeuf, F., Huot, J. and Gratton, J. P.** (2007). Src-mediated phosphorylation of Hsp90 in response to vascular endothelial growth factor (VEGF) is required for VEGF receptor-2 signaling to endothelial NO synthase. *Mol. Biol. Cell* **18**, 4659-4668.

**Ergun, S., Kilik, N., Ziegeler, G., Hansen, A., Nollau, P., Gotze, J., Wurmbach, J. H., Horst, A., Weil, J., Fernando, M. et al.** (2000). CEA-related cell adhesion molecule 1, a potent angiogenic factor and a major effector of vascular endothelial growth factor. *Mol. Cell* **5**, 311-320.

**Fournes, B., Farrah, J., Olson, M., Lamarche-Vane, N. and Beauchemin, N.** (2003). Distinct Rho GTPase activities regulate epithelial cell localization of the adhesion molecule CEACAM1: involvement of the CEACAM1 transmembrane domain. *Mol. Cell. Biol.* **23**, 7291-7304.

**Fukumura, D., Yuan, F., Endo, M. and Jain, R. K.** (1997). Role of nitric oxide in tumor microcirculation. Blood flow, vascular permeability, and leukocyte-endothelial interactions. *Am. J. Pathol.* **150**, 713-725.

**Fulton, D., Gratton, J. P., McCabe, T. J., Fontana, J., Fujio, Y., Walsh, K., Franke, T. F., Papapetropoulos, A. and Sessa, W. C.** (1999). Regulation of endothelium-derived nitric oxide production by the protein kinase Akt. *Nature* **399**, 597-601.

**Gray-Owen, S. D. and Blumberg, R. S.** (2006). CEACAM1: contact-dependent control of immunity. *Nat. Rev Immunol.* **6**, 433-446.

**He, H., Venema, V. J., Gu, X., Venema, R. C., Marrero, M. B. and Caldwell, R. B.** (1999). Vascular endothelial growth factor signals endothelial cell production of nitric oxide and prostacyclin through flk-1/KDR activation of c-Src. *J. Biol. Chem.* **274**, 25130-25135.

**Horst, A. K., Ito, W. D., Dabelstein, J., Schumacher, U., Sander, H., Turbide, C., Brummer, J., Meinertz, T., Beauchemin, N. and Wagener, C.** (2006). Carcinoembryonic antigen-related cell adhesion molecule 1 modulates vascular remodeling in vitro and in vivo. *J. Clin. Invest.* **116**, 1596-1605.

**Horst, A. K., Bickert, T., Brewig, N., Ludewig, P., van Rooijen, N., Schumacher, U., Beauchemin, N., Ito, W. D., Fleischer, B., Wagener, C. et al.** (2009). CEACAM1+ myeloid cells control angiogenesis in inflammation. *Blood* **113**, 6726-6736.

**Huber, M., Izzi, L., Grondin, P., Houde, C., Kunath, T., Veillette, A. and Beauchemin, N.** (1999). The carboxyl-terminal region of biliary glycoprotein controls its tyrosine phosphorylation and association with protein-tyrosine phosphatases SHP-1 and SHP-2 in epithelial cells. *J. Biol. Chem.* **274**, 335-344.

**Izzi, L., Turbide, C., Houde, C., Kunath, T. and Beauchemin, N.** (1999). cis-Determinants in the cytoplasmic domain of CEACAM1 responsible for its tumor inhibitory function. *Oncogene* **18**, 5563-5572.

**Jones, G. T., Jiang, F., McCormick, S. P. and Dusting, G. J.** (2005). Elastic lamina defects are an early feature of aortic lesions in the apolipoprotein E knockout mouse. *J. Vasc. Res.* **42**, 237-246.

**Kilic, N., Oliveira-Ferrer, L., Wurmbach, J. H., Loges, S., Chalajour, F., Neshat-Vahid, S., Weil, J., Fernando, M. and Ergun, S.** (2005). Pro-angiogenic signaling by the endothelial presence of CEACAM1. *J. Biol. Chem.* **280**, 2361-2369.

**Kilic, N., Oliveira-Ferrer, L., Neshat-Vahid, S., Irmak, S., Obst-Pernberg, K., Wurmbach, J. H., Loges, S., Kilic, E., Weil, J., Lauke, H. et al.** (2007). Lymphatic reprogramming of microvascular endothelial cells by CEA-related cell adhesion molecule-1 via interaction with VEGFR-3 and Prox1. *Blood* **110**, 4223-4233.

**Klaile, E., Vorontsova, O., Sigmundsson, K., Muller, M. M., Singer, B. B., Ofverstedt, L. G., Svensson, S., Skoglund, U. and Obrink, B.** (2009). The CEACAM1 N-terminal Ig domain mediates cis- and trans-binding and is essential for allosteric rearrangements of CEACAM1 microclusters. *J. Cell Biol.* **187**, 553-567.

**Kroll, J. and Waltenberger, J.** (1997). The vascular endothelial growth factor receptor KDR activates multiple signal transduction pathways in porcine aortic endothelial cells. *J. Biol. Chem.* **272**, 32521-32527.

**Lee, K., Forudi, F., Saidel, G. M. and Penn, M. S.** (2005). Alterations in internal elastic lamina permeability as a function of age and anatomical site precede lesion development in apolipoprotein E-null mice. *Circ. Res.* **97**, 450-456.

**Lee, S. J., Heinrich, G., Fedorova, L., Al-Share, Q. Y., Ledford, K. J., Fernstrom, M. A., McInerney, M. F., Erickson, S. K., Gatto-Weis, C. and Najjar, S. M.** (2008). Development of nonalcoholic steatohepatitis in insulin-resistant liver-specific S503A carcinoembryonic antigen-related cell adhesion molecule 1 mutant mice. *Gastroenterology* **135**, 2084-2095.

**Leung, N., Turbide, C., Olson, M., Marcus, V., Jothy, S. and Beauchemin, N.** (2006). Deletion of the carcinoembryonic antigen-related cell adhesion molecule 1 (Ceacam1) gene contributes to colon tumor progression in a murine model of carcinogenesis. *Oncogene* **25**, 5527-5536.

**Lobo, E. O., Zhang, Z. and Shively, J. E.** (2009). CEACAM1 is a negative coreceptor for the B cell receptor and promotes CD19-mediated adhesion of B cells in a PI3K-dependent manner. *J. Leukoc. Biol.* **86**, 205-218.

**Montagnani, M., Chen, H., Barr, V. A. and Quon, M. J.** (2001). Insulin-stimulated activation of eNOS is independent of Ca2+ but requires phosphorylation by Akt at Ser(1179). *J. Biol. Chem.* **276**, 30392-30398.

**Muller, M. M., Singer, B. B., Klaile, E., Obrink, B. and Lucka, L.** (2005). Transmembrane CEACAM1 affects integrin-dependent signaling and regulates extracellular matrix protein-specific morphology and migration of endothelial cells. *Blood* **105**, 3925-3934.

**Muller, M. M., Klaile, E., Vorontsova, O., Singer, B. B. and Obrink, B.** (2009). Homophilic adhesion and CEACAM1-S regulate dimerization of CEACAM1-L and recruitment of SHP-2 and c-Src. *J. Cell Biol.* **187**, 569-581.

**Nagaishi, T., Pao, L., Lin, S. H., Iijima, H., Kaser, A., Qiao, S. W., Chen, Z., Glickman, J., Najjar, S. M., Nakajima, A. et al.** (2006). SHP1 phosphatase-dependent T cell inhibition by CEACAM1 adhesion molecule isoforms. *Immunity* **25**, 769-781.

**Nagy, J. A., Benjamin, L., Zeng, H., Dvorak, A. M. and Dvorak, H. F.** (2008). Vascular permeability, vascular hyperpermeability and angiogenesis. *Angiogenesis* **11**, 109-119.

**Najjar, S. M.** (2002). Regulation of insulin action by CEACAM1. *Trends Endocrinol. Metab.* **13**, 240-245.

**Nakagami, H., Cui, T. X., Iwai, M., Shiuchi, T., Takeda-Matsubara, Y., Wu, L. and Horiuchi, M.** (2002). Tumor necrosis factor-alpha inhibits growth factor-mediated cell proliferation through SHP-1 activation in endothelial cells. *Arterioscler. Thromb. Vasc. Biol.* **22**, 238-242.

**Nouvion, A. L. and Beauchemin, N.** (2009). CEACAM1 as a central modulator of metabolism, tumor progression, angiogenesis and immunity. *Med. Sci.* **25**, 247-252.

**Olsson, A. K., Dimberg, A., Kreuger, J. and Claesson-Welsh, L.** (2006). VEGF receptor signalling-in control of vascular function. *Nat. Rev. Mol. Cell Biol.* **7**, 359-371.

**Pantelic, M., Kim, Y. J., Bolland, S., Chen, I., Shively, J. and Chen, T.** (2005). Neisseria gonorrhoeae kills carcinoembryonic antigen-related cellular adhesion molecule 1 (CD66a)-expressing human B cells and inhibits antibody production. *Infect. Immunol.* **73**, 4171-4179.

**Potenza, M. A., Addabbo, F. and Montagnani, M.** (2009). Vascular actions of insulin with implications for endothelial dysfunction. *Am. J. Physiol. Endocrinol. Metab.* **297**, E568-E577.

**Poy, M. N., Yang, Y., Rezaei, K., Fernstrom, M. A., Lee, A. D., Kido, Y., Erickson, S. K. and Najjar, S. M.** (2002). CEACAM1 regulates insulin clearance in liver. *Nat. Genet.* **30**, 270-276.

**Sadekova, S., Lamarche-Vane, N., Li, X. and Beauchemin, N.** (2000). The CEACAM1-L glycoprotein associates with the actin cytoskeleton and localizes to cell-cell contact through activation of Rho-like GTPases. *Mol. Biol. Cell* **11**, 65-77.

**Seo, D. W., Li, H., Guedez, L., Wingfield, P. T., Diaz, T., Salloum, R., Wei, B. Y. and Stetler-Stevenson, W. G.** (2003). TIMP-2 mediated inhibition of angiogenesis: an MMP-independent mechanism. *Cell* **114**, 171-180.

**Sessa, W. C.** (2004). eNOS at a glance. *J. Cell Sci.* **117**, 2427-2429.

**Sessa, W. C., Garcia-Cardena, G., Liu, J., Keh, A., Pollock, J. S., Bradley, J., Thiru, S., Braverman, I. M. and Desai, K. M.** (1995). The Golgi association of endothelial nitric oxide synthase is necessary for the efficient synthesis of nitric oxide. *J. Biol. Chem.* **270**, 17641-17644.

**Skubitz, K. M., Campbell, K. D., Ahmed, K. and Skubitz, A. P.** (1995). CD66 family members are associated with tyrosine kinase activity in human neutrophils. *J. Immunol.* **155**, 5382-5390.

**Slevogt, H., Zabel, S., Opitz, B., Hocke, A., Eitel, J., N'Guessan, P. D., Lucka, L., Riesbeck, K., Zimmermann, W., Zweigner, J. et al.** (2008). CEACAM1 inhibits Toll-like receptor 2-triggered antibacterial responses of human pulmonary epithelial cells. *Nat. Immunol.* **9**, 1270-1278.

**Thurston, G., Suri, C., Smith, K., McClain, J., Sato, T. N., Yancopoulos, G. D. and McDonald, D. M.** (1999). Leakage-resistant blood vessels in mice transgenically overexpressing angiopoietin-1. *Science* **286**, 2511-2514.

**Tilki, D., Irmak, S., Oliveira-Ferrer, L., Hauschild, J., Miethe, K., Atakaya, H., Hammerer, P., Friedrich, M. G., Schuch, G., Galalae, R. et al.** (2006). CEA-related cell adhesion molecule-1 is involved in angiogenic switch in prostate cancer. *Oncogene* **25**, 4965-4974.

**Xu, E., Dubois, M. J., Leung, N., Charbonneau, A., Turbide, C., Avramoglu, R. K., Demarte, L., Elchebly, M., Streichert, T., Levy, E. et al.** (2009). Targeted disruption of carcinoembryonic antigen-related cell adhesion molecule 1(Ceacam1) promotes diet-induced hepatic steatosis and insulin resistance. *Endocrinology* **150**, 3508-3512.

**Zengin, E., Chalajour, F., Gehling, U. M., Ito, W. D., Treede, H., Lauke, H., Weil, J., Reichenspurner, H., Kilic, N. and Ergun, S.** (2006). Vascular wall resident progenitor cells: a source for postnatal vasculogenesis. *Development* **133**, 1543-1551.